Analysis of the exciton-exciton interaction in semiconductor quantum wells

Christoph Schindler* and Roland Zimmermann
Institut für Physik, Humboldt-Universität zu Berlin, Newtonstraße 15, 12489 Berlin, Germany
(Received 22 February 2008; revised manuscript received 10 June 2008; published 15 July 2008)

The exciton-exciton interaction is investigated for quasi-two-dimensional quantum structures. A bosonization scheme is applied including the full spin structure. For generating the effective interaction potentials, the Hartree-Fock and Heitler-London approaches are improved by a full two-exciton calculation which includes the van der Waals effect. With these potentials the biexciton formation in bilayer systems is investigated. For coupled quantum wells the two-body scattering matrix is calculated and employed to give a modified relation between exciton density and blueshift. Such a relation is of central importance for gauging exciton densities in experiments which pave the way toward Bose-Einstein condensation of excitons.

DOI: 10.1103/PhysRevB.78.045313 PACS number(s): 73.20.Mf, 71.35.Gg, 78.67.De

I. INTRODUCTION

Excitons (bound pairs of electron and hole) play a key role in semiconductor optics, and their theoretical understanding has a long history.[1] Although excitons obey Bose statistics, the fermionic structure of their constituents is always important and forbids to treat excitons as nearly ideal Bose particles. Among the first attempts for bosonization of excitons, we quote Refs. 2–4. Both the fermionic exchange and the Coulomb forces between two excitons can be condensed into an effective exciton-exciton (XX) interaction potential. Efforts for deriving XX potentials are abound in the literature, covering three-dimensional excitons in bulk semiconductors as well as quasi-two-dimensional excitons in quantum wells. However, almost all of these attempts[5–8] were restricted to the Hartree-Fock level, i.e., taking into account the XX interactions up to second order in the elementary charge, e^2. Sometimes it has been claimed that this would be enough for treating sufficiently accurate the exciton gas at low density n_X. This is not correct since already at zero density, the single-exciton bound state calls for an infinite summation in powers of the Coulomb potential, and consequently the next term (linear in n_X) cannot be truncated either. It was not before 2001 that in a seminal paper by Okumura and Ogawa[9] the first XX potential beyond Hartree-Fock[10] for bulk semiconductors has been constructed, in close analogy to the Heitler-London approximation in atomic physics.

The interest in a proper description of XX interactions has been surely intensified by the actual search for Bose-Einstein condensation of excitons, which has been predicted theoretically already decades ago.[11–13] Due to the small exciton mass compared to atomic systems, the critical temperature for the condensate is expected to be a few kelvins for a density of 10^{17} cm^{-3} in bulk GaAs within easy reach experimentally. A fundamental problem, however, is the finite lifetime of the excitons, which hinders the relaxation into thermal equilibrium. One possible way out are coupled quantum wells (CQWs) which came into focus a few years ago.[14–18] A static electric field in growth direction forces electrons and holes to reside in adjacent quantum wells which are separated by a barrier. Due to this spatial separation, the indirect excitons exhibit extremely long lifetimes, which is a good condition for reaching thermal equilibrium. However, these spatially indirect excitons form dipoles leading to a strong and long-range repulsion, which complicates the theoretical description as well as the experimental realization of a dense cold exciton gas.[19,20] Recently large progress has been reported for spatially indirect excitons in electrostatic[21] as well as optical traps.[22,23]

These practical demands led us to investigate the XX interaction in more detail with special emphasis on coupled quantum wells. In particular, we improve on the Heitler-London-type treatment in Ref. 9 by solving the four-particle Schrödinger equation for two electrons and two holes numerically. Before doing so we address the complex spin structure of the exciton composed of a spin 1/2 electron and a spin 3/2 heavy hole (Sec. II). The importance of spin-dependent effects in the exciton gas has been emphasized, e.g., in Ref. 24. In the limit of immobile holes (their mass being usually much larger than that of the electrons), we can derive effective spin-dependent XX potentials (Sec. III), which contain in addition to the dipole-dipole repulsion and exchange effects the weak van der Waals forces. The latter is of importance to rectify a recent claim[25,26] to have explained the bead pattern formation which appears at low temperatures in the ring-shaped CQW emission.[27–29]

With a proper XX interaction at hand, we are able to calculate biexciton states (excitonic molecules), which are well known from bulk semiconductors and have been observed in single quantum wells.[30,31] Since biexciton energies have been calculated with high precision elsewhere,[32] we use these results to judge our approximate treatment in Sec. IV. For the CQW situation simplified to a bilayer system, we identify the parameter values (essentially mass ratio and charge separation) which limit the existence of biexcitons.

Addressing the many-exciton case, we will treat the excitons as effective bosons with a renormalized interaction potential, derived from the underlying electron-hole description.[33] As an application, we investigate in Sec. V two realistic CQW structures. The numerically generated XX potentials are used to calculate two-exciton scattering phase shifts which are the main ingredient for a T-matrix based quasiparticle dispersion.[34] For the low-density case, we are able to calculate excitonic blueshift and scattering-induced broadening linear in n_X (Sec. VI). We find a stunning reduction of the blueshift compared to the simple "capacitor for-

mula" and relate this finding to features in the XX pair-correlation function, which—due to the strong repulsion—resembles more a Fermi gas than a free Bose gas (Sec. VII). Conclusions are drawn in Sec. VIII, while a few technical details are deferred to the Appendix.

II. MANY-EXCITON HAMILTONIAN

To derive the many-exciton Hamiltonian we follow the work of de-Leon and Laikhtman.[8,35] The task is to find the matrix elements of the electron-hole Hamiltonian with an appropriate two-exciton wave function and to implement them into an effective bosonic Hamiltonian for many excitons. The effective-mass Hamiltonian for two electrons and holes reads

$$H_{2eh} = -\frac{\hbar^2\Delta_{e1}}{2m_e} - \frac{\hbar^2\Delta_{h1}}{2m_h} - \frac{\hbar^2\Delta_{e2}}{2m_e} - \frac{\hbar^2\Delta_{h2}}{2m_h} + v_{ee}(\mathbf{r}_{e1}-\mathbf{r}_{e2}) + v_{hh}(\mathbf{r}_{h1}-\mathbf{r}_{h2}) - v_{eh}(\mathbf{r}_{e1}-\mathbf{r}_{h1}) - v_{eh}(\mathbf{r}_{e2}-\mathbf{r}_{h2}) - v_{eh}(\mathbf{r}_{e1}-\mathbf{r}_{h2}) - v_{eh}(\mathbf{r}_{e2}-\mathbf{r}_{h1}), \quad (1)$$

where the interaction part [fifth to tenth terms of Eq. (1)] is composed of Coulomb interactions between particle a and b, which can be either electron ($a=e$) or hole ($a=h$),

$$v_{ab}(\mathbf{r}) = \frac{e_0^2}{r} \quad \text{with} \quad e_0^2 = \frac{e^2}{4\pi\epsilon_0\epsilon_s}. \quad (2)$$

Please note that the corresponding sign (attractive or repulsive) has been made explicit in Eq. (1).

We define exciton quantum field operators $\Psi_s^\dagger(\mathbf{R})$, which create an exciton at exciton center-of-mass (c.m.) position $\mathbf{R}$ with spin s, and $\Psi_s(\mathbf{R})$, which annihilates the same exciton. The subsequent Hamilton operator can be written as

$$H_{XX} = \int d\mathbf{R} \sum_s \Psi_s^\dagger(\mathbf{R}) \frac{-\hbar^2\Delta_{\mathbf{R}}}{2M} \Psi_s(\mathbf{R}) + \frac{1}{2}\int d\mathbf{R} d\mathbf{R}' \sum_{s1s2s3s4} W_{s1s2,s3s4}(\mathbf{R}-\mathbf{R}') \times \Psi_{s1}^\dagger(\mathbf{R})\Psi_{s2}^\dagger(\mathbf{R}')\Psi_{s3}(\mathbf{R}')\Psi_{s4}(\mathbf{R}), \quad (3)$$

with the exciton mass $M=m_e+m_h$ in the kinetic energy. $W_{s1s2,s3s4}(\mathbf{R})$ is the spin and space-dependent pair interaction potential. In the following, it will be extracted from a careful study of the four-particle problem [Eq. (1)]. The exciton spin index $s=s_e+J_h$ is the sum of the electron spin ($s_e=\pm 1/2$) and the heavy-hole angular momentum ($J_h=\pm 3/2$). We neglect the light holes, which are separated due to the confinement effects in the quasi-two-dimensional quantum well (QW). Now, s runs over four values $s=\pm 1$ (bright states) and $s=\pm 2$ (dark states). Since electron and hole are fermions, we have to use a properly symmetrized ansatz for both component's spin wave functions $\chi_{ee}^p(s_{e1},s_{e2})$ and $\chi_{hh}^q(J_{h1},J_{h2})$, which make the overall wave-function antisymmetric with respect to the exchange of the electrons and the holes, respectively. The labels p and q denote the parity which can be symmetric ($p=s$) or antisymmetric ($p=a$). Together with the spatial part we write the total two-exciton wave function,

TABLE I. Spin structure of the exciton-exciton interaction $W_{s1s2,s3s4}(\mathbf{R})$ in quantum wells.

	$\lvert 2,2\rangle$	$\lvert 1,1\rangle$	$\lvert -1,-1\rangle$	$\lvert -2,-2\rangle$	$\lvert 2,-1\rangle$	$\lvert -1,2\rangle$	$\lvert 1,-2\rangle$	$\lvert -2,1\rangle$
$\langle 2,2\rvert$	U_a^a							
$\langle 1,1\rvert$		U_a^a					0	
$\langle -1,-1\rvert$			U_a^a					
$\langle -2,-2\rvert$				U_a^a				
$\langle 2,-1\rvert$					U_+^a	U_-^a		
$\langle -1,2\rvert$		0			U_-^a	U_+^a		
$\langle 1,-2\rvert$							U_+^a	U_-^a
$\langle -2,1\rvert$							U_-^a	U_+^a

	$\lvert 1,2\rangle$	$\lvert 2,1\rangle$	$\lvert -2,-1\rangle$	$\lvert -1,-2\rangle$	$\lvert 2,-2\rangle$	$\lvert 1,-1\rangle$	$\lvert -2,2\rangle$	$\lvert -1,1\rangle$
$\langle 1,2\rvert$	U_a^+	U_a^-						
$\langle 2,1\rvert$	U_a^-	U_a^+					0	
$\langle -2,-1\rvert$			U_a^+	U_a^-				
$\langle -1,-2\rvert$			U_a^-	U_a^+				
$\langle 2,-2\rvert$					U_+^+	U_+^-	U_-^-	U_-^+
$\langle 1,-1\rvert$		0			U_+^-	U_+^+	U_-^+	U_-^-
$\langle -2,2\rvert$					U_-^-	U_-^+	U_+^+	U_+^-
$\langle -1,1\rvert$					U_-^+	U_-^-	U_+^-	U_+^+

$$\Psi_q^p(\mathbf{r}_{e1},s_{e1},\mathbf{r}_{e2},s_{e2},\mathbf{r}_{h1},J_{h1},\mathbf{r}_{h2},J_{h2}) = \psi_q^p(\mathbf{r}_{e1},\mathbf{r}_{e2},\mathbf{r}_{h1},\mathbf{r}_{h2})\chi_{ee}^{-p}(s_{e1},s_{e2})\chi_{hh}^{-q}(J_{h1},J_{h2}), \quad (4)$$

where the upper label stands for the electron part, and the lower one for the hole part. Please note that due to the fermionic nature of the particles, the parities of the spin part and of the spatial part have to be opposite to each other. Taking now the matrix elements of Eq. (1) with the ground-state wave functions, we get four different potentials,[36]

$$U_q^p = \langle \Psi_q^p | H_{2eh}^{\text{int}} | \Psi_q^p \rangle. \quad (5)$$

Due to the one to one correspondence between the exciton spin and the spin of its constituents, it is possible to express the basis vectors in the space of symmetric and antisymmetric spin wave functions by the spin eigenstates of the excitons $|s_1,s_2\rangle$. After a straightforward unitary transformation one gets the interaction matrix elements $W_{s1s2,s3s4}(\mathbf{R})$ as shown in Table I for columns $|s_3s_4\rangle$ and rows $\langle s_1s_2|$. Here $U_q^\pm = 1/2(U_q^a \pm U_q^s)$ and similar for the lower hole index. We can clearly see the block structure of the interaction which reflects the conservation of the total spin $s_1+s_2=s_3+s_4$. The interaction channels can be classified as follows: There is the direct channel where an initial state $|s_1,s_2\rangle$ will remain unchanged. The other channel is of exchange type with a change in the initial state due to three different processes: Exchange of electrons, exchange of holes, and exchange of both simultaneously. The electron-hole exchange process (longitudinal-transverse splitting of the exciton) has been neglected already in the starting Hamiltonian.

In a case where the hole mass is much larger than the electron mass, the exchange of holes becomes negligible and the four different potentials [Eq. (5)] collapse into two, $U^a = U_q^a$ and $U^s = U_q^s$, which correspond to wave functions properly symmetrized only with respect to the electrons. In this case the interaction part of the Hamiltonian simplifies to the form shown in Table II where $U^\pm = 1/2(U^a \pm U^s)$ and can be cast into the form given in the Appendix [Eq. (A1)].

TABLE II. Spin structure of the exciton-exciton interaction $W_{s1s2,s3s4}(\mathbf{R})$ in the case of infinitely heavy holes.

	$\|2,2\rangle$	$\|1,1\rangle$	$\|-1,-1\rangle$	$\|-2,-2\rangle$	$\|2,-1\rangle$	$\|-1,2\rangle$	$\|1,-2\rangle$	$\|-2,1\rangle$
$\langle 2,2\|$	U^a							
$\langle 1,1\|$		U^a					0	
$\langle -1,-1\|$			U^a					
$\langle -2,-2\|$				U^a				
$\langle 2,-1\|$					U^a			
$\langle -1,2\|$		0				U^a		
$\langle 1,-2\|$							U^a	
$\langle -2,1\|$								U^a

	$\|1,2\rangle$	$\|2,1\rangle$	$\|-2,-1\rangle$	$\|-1,-2\rangle$	$\|2,-2\rangle$	$\|1,-1\rangle$	$\|-2,2\rangle$	$\|-1,1\rangle$
$\langle 1,2\|$	U^+	U^-						
$\langle 2,1\|$	U^-	U^+					0	
$\langle -2,-1\|$			U^+	U^-				
$\langle -1,-2\|$			U^-	U^+				
$\langle 2,-2\|$					U^+	U^-		
$\langle 1,-1\|$		0			U^-	U^+		
$\langle -2,2\|$							U^+	U^-
$\langle -1,1\|$							U^-	U^+

III. EFFECTIVE INTERACTION POTENTIALS

To derive the spatial dependence of the interaction potentials introduced in Sec. II, approximations have been introduced in the literature. In the infinitely heavy-hole limit, the Heitler-London ansatz is well known from atomic physics and has recently been brought into exciton physics by Okumura and Ogawa.[9] In a bulk semiconductor, the two excitons resemble a hydrogen molecule in this limit. The problem of four particles (two electrons and two holes) simplifies here to a two-particle problem for the electrons, while the hole-hole distance $\mathbf{R}$ enters as a parameter. Therefore, the Coulomb potential between the holes gives just a fixed additional term in the Hamiltonian. The two-exciton wave function can then be written as a properly antisymmetrized product of single-exciton wave functions in the $1s$ ground state $\phi(\mathbf{r})$, centered around the position of each hole. For the spatial part of the two-exciton wave function, we can write

$$\psi^{s,a}(\mathbf{r}_1,\mathbf{r}_2) = \frac{1}{\sqrt{2}} \frac{\phi(\mathbf{r}_1)\phi(\mathbf{r}_2-\mathbf{R}) \pm \phi(\mathbf{r}_1-\mathbf{R})\phi(\mathbf{r}_2)}{\sqrt{1 \pm \mathcal{O}^2(\mathbf{R})}}, \quad (6)$$

with the wave-function overlap,

$$\mathcal{O}(\mathbf{R}) = \int d\mathbf{r}\phi(\mathbf{r})\phi(\mathbf{r}-\mathbf{R}), \quad (7)$$

which leads to the potentials,

$$U^s(\mathbf{R}) = \frac{U_d(\mathbf{R}) - U_x(\mathbf{R})}{1+\mathcal{O}^2(\mathbf{R})},$$

$$U^a(\mathbf{R}) = \frac{U_d(\mathbf{R}) + U_x(\mathbf{R})}{1-\mathcal{O}^2(\mathbf{R})}, \quad (8)$$

with direct $U_d(\mathbf{R})$ and exchange $U_x(\mathbf{R})$ potential [explicit expressions are given in the Appendix, Eqs. (A4) and (A5)].

A simplified version of the Heitler-London approximation, which has usually been applied to excitonic systems,[5,6,8,37] is the famous Hartree-Fock treatment where the normalization denominator in Eq. (6) is left out and is consequently missing in Eq. (8). This scheme can easily be generalized to arbitrary hole masses. However, it leads to a nonlocal exchange potential[5] and to problems with the orthogonality of the basis states.[38]

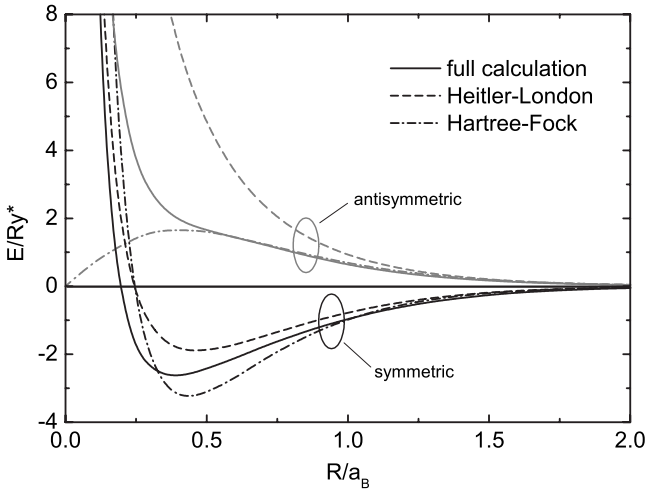

FIG. 1. Effective interaction potentials for the strictly two-dimensional system: full calculation results (solid lines), Heitler-London approximation (dashed lines), and Hartree-Fock approximation (dot-dashed lines) plotted vs distance in units of the three-dimensional (3D) (bulk) exciton Bohr radius a_B. The vertical axis is given in units of the bulk exciton Rydberg energy Ry^*. Antisymmetric channels are displayed in gray, while symmetric channels have black lines.

To improve over the approximations discussed so far, we have solved the Schrödinger equation for the two electrons numerically using the Lanczos algorithm, treating the holes as infinitely heavy and thus immobile. The equation to be solved reads

$$\left[-\frac{\hbar^2}{2\mu}(\Delta_{\mathbf{r}_1}+\Delta_{\mathbf{r}_2}) + v_{ee}(\mathbf{r}_2-\mathbf{r}_1) + v_{hh}(\mathbf{R}) - v_{eh}(\mathbf{r}_1) - v_{eh}(\mathbf{r}_2) - v_{eh}(\mathbf{r}_2-\mathbf{R}) - v_{eh}(\mathbf{r}_1-\mathbf{R})\right]\Psi^p(\mathbf{r}_1,\mathbf{r}_2) = [-2B_X + U^p(\mathbf{R})]\Psi^p(\mathbf{r}_1,\mathbf{r}_2), \quad (9)$$

where μ is the effective electron mass in the plane and B_X is the single-exciton binding energy. The zero of energy is chosen to be the band gap. Figure 1 shows the resulting effective interaction potentials in Hartree-Fock, Heitler-London, and full numerical quality exemplarily for a strictly two-dimensional system. We note the unphysical behavior of the Hartree-Fock antisymmetric potential which approaches zero for small distances. It also misses the proper sequence of the antisymmetric channel to be above the symmetric one for small distances. This is the result of leaving out the normalization denominator in Eq. (6). Thus these problems are corrected in the Heitler-London treatment. Here also the antisymmetric channel shows the expected Coulomb singularity of the hole-hole potential for small distances. In the full solution the energy is lowered compared to the Heitler-London approximation by a mutual deformation of the excitonic orbitals. Please note that the van der Waals effect is included due to the nonperturbative nature of the calculation.

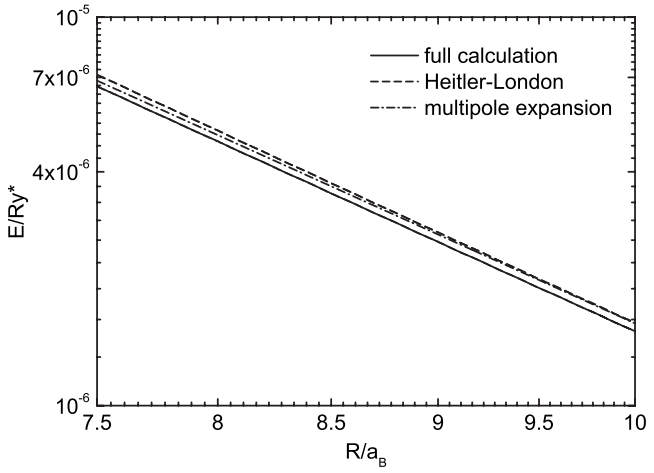

FIG. 2. Asymptotic behavior of the potentials on a double-logarithmic plot for the strictly two-dimensional system: full calculation (solid), Heitler-London (dashed), and multipole expansion (dot-dashed); symmetric states lie on top of antisymmetric ones.

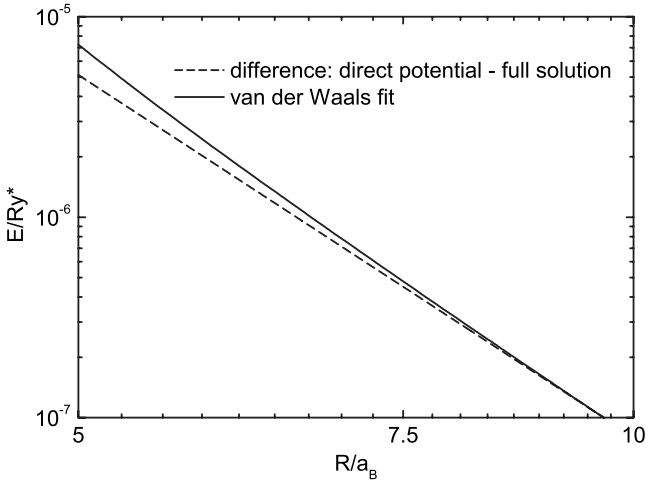

FIG. 3. The van der Waals effect in the strictly two-dimensional system. Deviation of the full calculation from the direct potential for asymptotic large distances (solid line) and fitted van der Waals like potential $\propto 1/R^6$ (dashed line).

While the considerations above are correct also in three dimensions, we turn now to the two-dimensional case of quantum structures. All vectors are to be understood as lying in the $x-y$ plane, the z axis being the growth direction. We note that all interaction potentials in Fig. 1 approach zero from positive values and hence show a repulsion for larger distances, although this is hardly seen in Fig. 1. However, this behavior follows already from a multipole expansion of the direct potential $U_d(\mathbf{R})$, which dominates the interaction at large distances. In such an approach we treat the exciton as a static charge distribution $\rho(\mathbf{r},z)$ with cylindrical symmetry and centered at zero c.m. coordinate. The specific form of $\rho(\mathbf{r},z)$ depends on the system under investigation and will be specified later. Due to the charge neutrality of the exciton the multipole expansion starts with the dipole term $\propto 1/R^3$, where $\mathbf{R}$ denotes the in-plane c.m. distance of the two excitons. Up to the quadrupole term, we obtain for the asymptotics

$$R \to \infty: U_d(\mathbf{R}) = \frac{e_0^2}{R^3}\langle z\rangle^2 + \frac{e_0^2}{R^5}\left(\frac{9}{4}\langle x^2 - z^2\rangle^2 + 3\langle z\rangle\langle z(3x^2 - z^2)\rangle\right), \tag{10}$$

where the angular brackets denote averaging over $\rho(\mathbf{r},z)$. For a bulk system with spherical symmetry we see immediately that the multipole expansion vanishes as expected. However, for the reduced symmetry of quasi-two-dimensional systems, we get finite multipoles also for in-plane circular symmetry. Even for the strictly two-dimensional system, where $z \equiv 0$, there is a contribution from the quadrupole-quadrupole interaction ($\propto 1/R^5$). This holds as well for symmetric single QWs where $\langle z\rangle = 0$ due to the mirror symmetry along the z axis. The direct interaction thus falls off as a power law rather than exponentially, which has been overlooked in a recent investigation of the asymptotic XX potential.[25] In Fig. 2 we compare the asymptotic behavior of the numerically calculated direct potential [Eq. (A4)], and the result from the multipole expansion [Eq. (10)] using the strictly two-dimensional charge distribution for an immobile hole $\rho(\mathbf{r},z) = \delta(z)[\delta(\mathbf{r}) - \phi^2(\mathbf{r})]$ and the usual Coulomb potentials [Eq. (2)]. The multipole expansion holds for $R \gtrsim 9a_B$. The full solution shows the van der Waals effect and lies below the direct potential. However, this effect is not able to overcome the repulsive nature of the asymptotic potential. To grasp this effect a bit more quantitatively, we plot in Fig. 3 the difference between the direct potential from the approximations of rigid orbitals and a corresponding quantity for the full solution $[U_d^{\text{full}} = 1/2(U^a + U^s)]$. For very large distances $R \gtrsim 10a_B$, we fit this difference to a van der Waals potential, i.e., $a \propto 1/R^6$ power law (dashed line in Fig. 3). The van der Waals law holds only for distances $R \gtrsim 9a_B$. For smaller distances higher-order effects come in and spoil the $\propto 1/R^6$ dependence.

With the derived effective interaction potentials, we construct the two-dimensional Schrödinger equation for two excitons with mutual distance R in c.m. space, where we introduce now the finite exciton mass $M = m_e + m_h$ in the kinetic term,

$$\left\{\frac{\hbar^2}{M}\left(-\frac{1}{R}\frac{d}{dR}R\frac{d}{dR} + \frac{m^2}{R^2}\right) + U^p(R)\right\}\psi_m^p(R) = E_m^p\psi_m^p(R), \tag{11}$$

where m denotes the angular quantum number. Please note the missing factor of 2 in the denominator of the kinetic term since we have to consider the reduced mass of two excitons, $\mu_X = M/2$.

IV. MODEL SYSTEMS

To test the reliability of our Born-Oppenheimer-type method, we calculate the biexciton binding energy B_{XX} from the lowest state of Eq. (11) with $m=0$ for different mass ratios $\sigma = m_e/m_h$ in the strictly two-dimensional limit. These

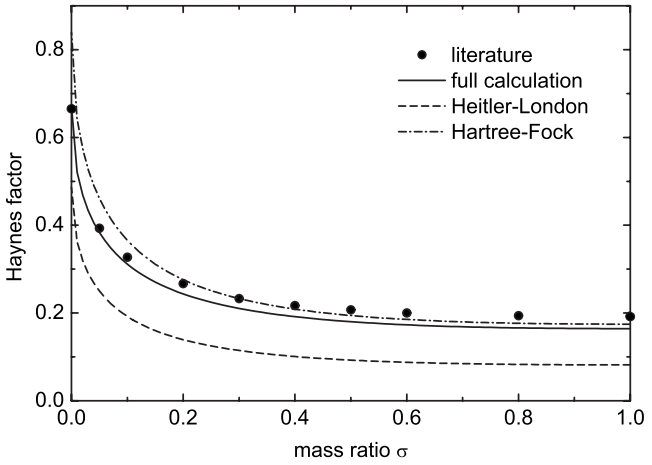

FIG. 4. Haynes factor $f_H=B_{XX}/B_X$ for the different potentials in the strictly two-dimensional system: full calculation (solid line), Heitler-London potential (dashed line), and Hartree-Fock potential (dot-dashed line) plotted vs mass ratio $\sigma=m_e/m_h$. The dots are numerically exact values from Ref. 32.

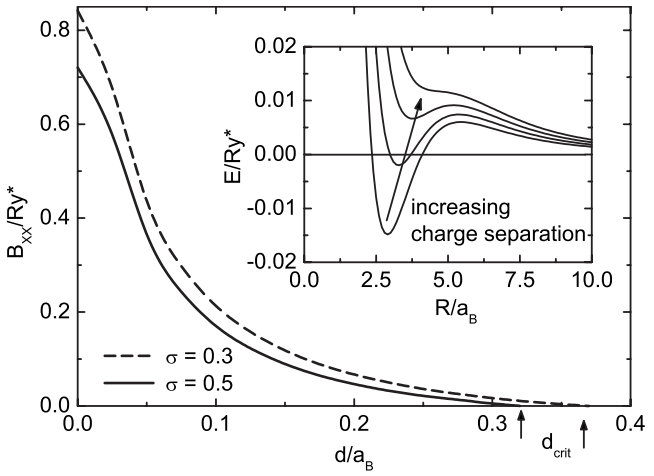

FIG. 5. Biexciton binding energy in the bilayer system plotted vs charge separation at $\sigma=0.5$ (solid line) and $\sigma=0.3$ (dashed line). The arrows denote the corresponding critical charge separation d_{crit}. Curves in the inset show the symmetric potential $U^s(R)$ for $d=0.8$, 0.9, 1.0, and 1.1 in units of the 3D exciton Bohr radius a_B.

results are compared in Fig. 4 with variational calculations from the literature[32] which are numerically exact. As expected, our method produces exact results for $\sigma=0$. For nonzero mass ratio we underestimate the binding energy slightly, e.g., for $\sigma=0.3$ we have an error of $\approx 8\%$. Even for $\sigma=1$ the error is only about 12%. We conclude that the method is a reasonable approximation for GaAs quantum structures ($\sigma=0.3$), which will be under investigation in Sec. V. We plot the Haynes factor $f_H=B_{XX}/B_X$ for the other approximations as well (for the strictly two-dimensional system, $B_X=4$ Ry*). The Heitler-London approximation underestimates the biexciton binding energy significantly. Hartree-Fock seems to do much better, but note that for small σ the Haynes factor is overestimated, which is in contrast to the variational principle.

A simple model for a coupled quantum well structure is the so-called bilayer system:[39] Electrons and holes are confined each in infinitely narrow planes with a separation d between the layers. This separation of unequal charges leads to a reduced Coulomb interaction between particles in different layers but leaves the potentials between particles of the same kind unchanged,

$$v_{eh}(\mathbf{r})=\frac{e_0^2}{\sqrt{r^2+d^2}},\quad v_{ee}(\mathbf{r})=v_{hh}(\mathbf{r})=\frac{e_0^2}{r}. \tag{12}$$

The charge distribution reads now $\rho(\mathbf{r},z)=\delta(z)\delta(\mathbf{r})-\delta(z-d)\phi^2(\mathbf{r})$, and the expansion [Eq. (10)] yields a finite dipole-dipole interaction $\propto 1/R^3$, resulting in a strong long-range repulsion. For the many-exciton problem we are in particular interested in the biexciton formation. Figure 5 shows the biexciton binding energy versus charge separation for a mass ratio of $\sigma=0.3$ and $\sigma=0.5$. In both cases we find a fast reduction in B_{XX} with increasing separation between the layers as expected. At a certain critical charge separation d_{crit}, denoted by the arrows in Fig. 5, the biexciton ceases to exist. The same model system has been investigated by Tan *et al.*[39] using quantum Monte Carlo (QMC) technique. From their results at intermediate values of d, which agree nicely with our own calculations, the authors suggested an exponential decay of B_{XX} for large d. The inset of Fig. 5 shows the potential in the symmetric channel for different values of the charge separation. It is clearly seen how the potential minimum passes through zero with increasing d and vanishes completely if d is enlarged further (large arrow). Therefore a (finite) critical charge separation d_{crit} exists where the biexciton binding energy becomes zero due to the dominant dipole-dipole repulsion. More recently this critical behavior was also observed in QMC calculations of Lee and Needs.[40] In Fig. 6 we plot the critical charge separation vs mass ratio. Below this curve, in the shaded area, bound states can be formed, while above no biexcitons exist. For small σ we obtain a rapid decrease in the critical charge separation. For larger mass ratios, on the other hand, the separation does not depend much on σ. This behavior resembles Fig. 4, revealing

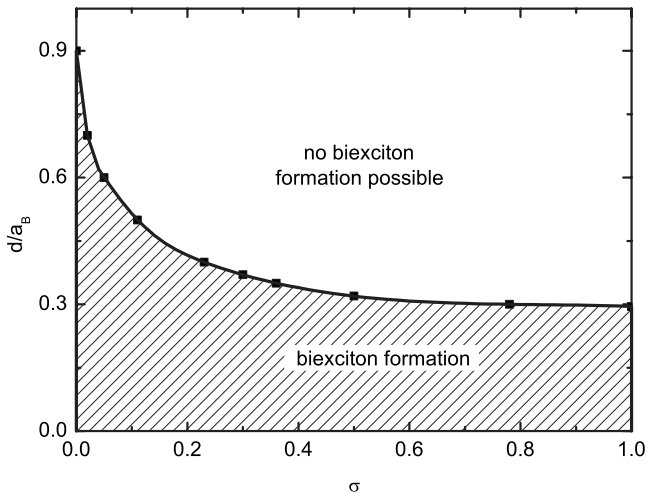

FIG. 6. Critical charge separation in units of the bulk exciton Bohr radius a_B plotted vs mass ratio $\sigma=m_e/m_h$.

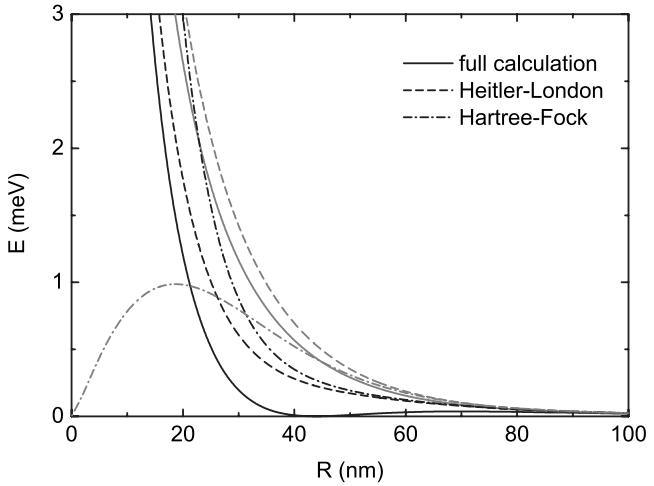

FIG. 7. Interaction potentials for sample A: full calculation results (solid lines), Heitler-London potentials (dashed lines), and Hartree-Fock potentials (dot-dashed lines) plotted vs distance. Antisymmetric channels have gray lines, while symmetric channels have black ones.

a direct connection between biexciton binding energy and critical charge separation.

V. RESULTS FOR COUPLED QUANTUM WELLS

We turn now to realistic coupled quantum well structures, having GaAs as well material and barriers made of $Al_xGa_{1-x}As$. In this case we treat the Coulomb interaction $v_{ab}(\mathbf{r})$ in single sublevel approximation,[33,41] which is given by

$$v_{ab}(\mathbf{r}) = e_0^2 \int dz' dz \frac{u_a^2(z') u_b^2(z'-z)}{\sqrt{r^2 + (z-z')^2}}. \tag{13}$$

Here, $\mathbf{r}$ is again an in-plane vector, and $u_e(z)$ and $u_h(z)$ denote the confinement functions of the lowest sublevel for electron and hole. They enter as well the static charge distribution of the exciton: $\rho(\mathbf{r},z) = u_h^2(z)\delta(\mathbf{r}) - u_e^2(z)\phi^2(\mathbf{r})$. Figure 7 shows the effective interaction potentials for a $GaAs/Al_{0.3}Ga_{0.7}As$ coupled quantum well geometry used by Butov[28] with a nominal (i.e., center distance between the wells) charge separation of $d=12$ nm (sample A in Table III). We see again the already discussed features of the three approximation levels. The energy gain when going from

TABLE III. Details of the used CQW geometry together with the calculated binding energy B_X of the indirect exciton.

	Sample A	Sample B
Well width L_z (nm)	8.0	10.0
Barrier width (nm)	4.0	4.0
d (nm)	12.0	14.0
d_{eff} (nm)	10.8	12.7
Static field (kV/cm)	30.0	36.0
B_X (meV)	4.0	3.5

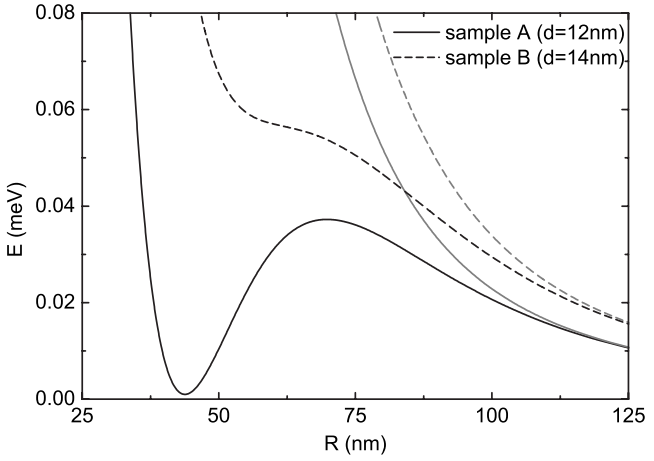

FIG. 8. Comparison of the full calculation results for sample A (solid lines) and sample B (dashed lines). Antisymmetric channels have gray lines, while symmetric channels have black ones.

Heitler-London to the full calculation yields a minimum for the symmetric channel, which however is so weak that no biexcitons can be formed. This feature strongly depends on the geometry of the quantum wells, which is illustrated in Fig. 8. Here the full calculation potentials for sample A are compared to another one used by Snoke *et al.*[42] where $d=14$ nm (sample B in Table III). Due to the larger charge separation no minimum can be seen in the symmetric channel. This observation is consistent with the results obtained for the idealized (bilayer) model discussed in Sec. IV.

With these results a simple explanation for the regular bead pattern in the luminescence ring at low temperatures[27–29] has to be ruled out: It was speculated[25,26] that the van der Waals effect could overcome the dipole-dipole repulsion, resulting in an attraction between spatially indirect excitons, which would lead to a spontaneous patterning. Our calculation shows that this is not the case in agreement with recent experimental investigations.[43,44] In Ref. 25 the quadrupole-quadrupole interaction in two-dimensional systems has been overlooked and hence the role of the van der Waals force overestimated as discussed in Sec. VI.

VI. EXCITON BLUESHIFT AND BROADENING

We turn now to the calculation of the interaction induced blueshift and broadening which can be observed in photoluminescence experiments.[42,45,46] In a point-charge treatment of spatially indirect excitons, we have from Eq. (A4)

$$U_d(\mathbf{R}) = v_{hh}(\mathbf{R}) + v_{ee}(\mathbf{R}) - 2v_{eh}(\mathbf{R}). \tag{14}$$

Plugging in Eq. (12) for the bilayer system, one gets a dipole-dipole repulsion of the form

$$U_d(\mathbf{R}) \approx e_0^2 \left[\frac{2}{R} - \frac{2}{\sqrt{R^2 + d^2}} \right]. \tag{15}$$

Assuming a homogeneous exciton density n_X, this leads to a blueshift,

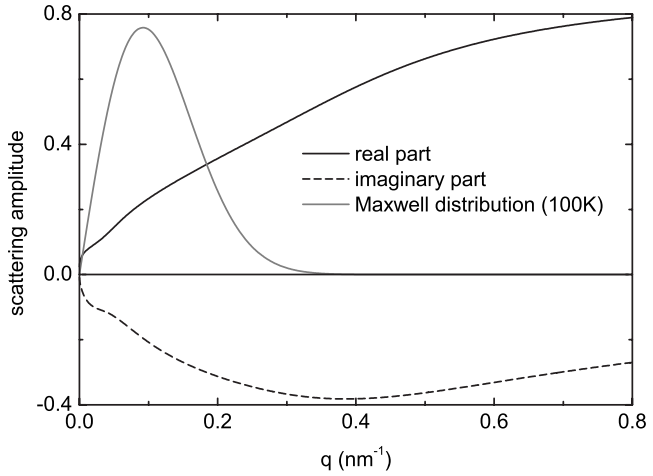

FIG. 9. Real (solid line) and imaginary (dashed line) parts of the scattering amplitude as a function of momentum for sample A. Included is the Maxwell distribution at $T=100$ K to show the relevant values for q. The ordinate has been normalized to the capacitor value [Eq. (16)].

$$\Delta_0 = \int d^2R U_d(\mathbf{R}) n_X = d\frac{e^2}{\epsilon_0 \epsilon_s} n_X. \tag{16}$$

Since this expression is consistent with the electrostatics of a plate capacitor, it is often referred to as capacitor formula.[47] We will derive a corrected formula for the blueshift and the scattering-induced broadening using the effective interaction potentials given in Fig. 8. The exciton self-energy is calculated in a T-matrix approach.[34] In the low-density limit and assuming complete spin equilibrium, we write the two-body T-matrix equation as

$$\langle \mathbf{q}|T^p(z)|\mathbf{q}''\rangle = U^p_{\mathbf{q}-\mathbf{q}''} - \sum_{\mathbf{q}'} \frac{U^p_{\mathbf{q}-\mathbf{q}'}}{2\epsilon_{\mathbf{q}'} - \hbar z} \langle \mathbf{q}'|T^p(z)|\mathbf{q}''\rangle. \tag{17}$$

The T-matrix enters the quasiparticle self-energy as boson direct (D) and boson exchange (X),

$$\Sigma_{\mathbf{k}}(\epsilon_{\mathbf{k}}) = 4\sum_{\mathbf{q}} \{\langle \mathbf{q}|T^D(z)|\mathbf{q}\rangle + \langle \mathbf{q}|T^X(z)|-\mathbf{q}\rangle\} \times n_B\left(\frac{\hbar^2}{2M}(\mathbf{k}+2\mathbf{q})^2 - \mu\right), \tag{18}$$

where $\hbar z = \hbar^2 q^2/M + i0$ is put on shell and $n_B(\epsilon)$ is the exciton distribution function, which is later taken as the low-density Maxwell-Boltzmann expression. The spin structure of the Hamiltonian yields the following decomposition in the limit of immobile holes:

$$T^D = 3T^a + T^s \quad \text{and} \quad T^X = 3/2T^a - 1/2T^s. \tag{19}$$

The on-shell T-matrix needed in Eq. (18) depends exclusively on the phase shifts $\delta^p_m(q)$ via[48]

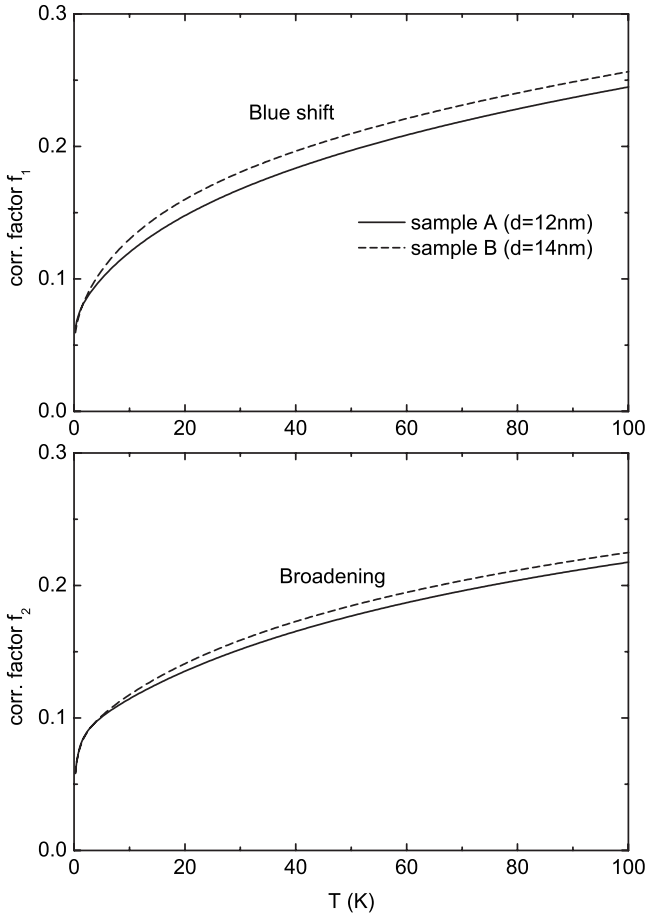

FIG. 10. Correction factors to the capacitor formula in dependence on temperature for sample A (solid lines) and sample B (dashed lines). The upper panel shows f_1 (blueshift), while the lower one shows f_2 (broadening).

$$\langle \mathbf{q}|T^p(z)|\pm\mathbf{q}\rangle = \frac{\hbar^2}{M}\sum_m (\pm 1)^m \frac{4}{i - \cot[\delta^p_m(q)]}. \tag{20}$$

We have extracted the phase shifts from the asymptotics of the solution of the radial Schrödinger equation [Eq. (11)] for $E=\hbar^2q^2/M$. Results for the total complex scattering amplitude [curly brackets in Eq. (18)] are shown in Fig. 9. Please note that for large momenta q, the real part of the scattering amplitude approaches the prediction of the capacitor formula but with an effective charge separation d_{eff} which is somewhat below the nominal one (third and forth rows of Table III). This reduction is due to the spatial extension of electron and hole charges along z. A simple argument assuming confinement wave functions for infinite barriers leads to $d_{\text{eff}} \approx d - 0.1267\ L_z$. This is quite close to the numerical value which follows from replacing the point-charge potential [Eq. (15)] in Eq. (16) by the numerically derived one.

Using the scattering amplitude, we calculate the quasiparticle shift and broadening at the dispersion edge ($\mathbf{k}=0$) and introduce correction factors $f_1(T)$ and $f_2(T)$ to the capacitor formula

$$\sum_0(0) = d\frac{e^2}{\epsilon_0\epsilon_S}n_X[f_1(T) - if_2(T)]. \quad (21)$$

The real part of this quantity is the blueshift Δ of the exciton due to the repulsive interaction, while the imaginary part can be associated with a finite broadening. Please note that with the sign convention used, Im Σ is negative. The correction factors shown in Fig. 10 reduce the capacitor result dramatically. Therefore, the density for a measured blueshift would be underestimated by a factor of 10 at low temperatures. The broadening is of the same order of magnitude, which is consistent with experimental findings.

VII. EXCITON-EXCITON CORRELATION FUNCTION

The significant reduction of the quasiparticle shift compared to the capacitor value can be explained with a strong depletion of the exciton gas around a given exciton due to the repulsive interaction. To grasp this repulsive correlation more directly we calculate the exciton pair-correlation function,

$$g_{ss'}(\mathbf{R}) = \frac{\langle\Psi_s^\dagger(\mathbf{R})\Psi_{s'}^\dagger(0)\Psi_{s'}(0)\Psi_s(\mathbf{R})\rangle}{\langle\Psi_s^\dagger(\mathbf{R})\Psi_s(\mathbf{R})\rangle\langle\Psi_{s'}^\dagger(0)\Psi_{s'}(0)\rangle}$$

$$= \frac{1}{n_s n_{s'}}\sum_{\mathbf{kk'q}} e^{i\mathbf{qR}}\langle\Psi_{\mathbf{k}s}^\dagger\Psi_{\mathbf{k'+q}s'}^\dagger\Psi_{\mathbf{k'}s'}\Psi_{\mathbf{k+q}s}\rangle. \quad (22)$$

It has the same spin structure as the T matrix. In the spin equilibrated situation investigated here, the exciton density n_s does not depend on spin. Summing over both spin indices, we obtain with a partial-wave decomposition,

$$g(\mathbf{R}) = \frac{\sum_{\mathbf{k},m}\exp\left(-\frac{\hbar^2k^2}{Mk_BT}\right)\left\{3|\psi_m^a(R)|^2 + |\psi_m^s(R)|^2 + (-1)^m\left(\frac{3}{2}|\psi_m^a(R)|^2 - \frac{1}{2}|\psi_m^s(R)|^2\right)\right\}}{4\sum_{\mathbf{k}}\exp\left(-\frac{\hbar^2k^2}{Mk_BT}\right)}. \quad (23)$$

The results shown in Fig. 11 reflect the strong repulsion of the excitons independent of the spin channel. It is interesting to compare with the pair-correlation function of ideal bosons and fermions having four spin degrees of freedom as well. Obviously in the present case, the repulsive interaction between excitons is much more important than the bosonic nature of their statistics.

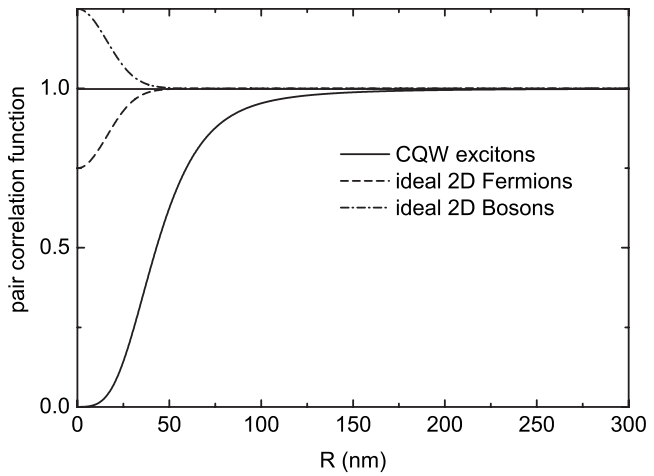

FIG. 11. Exciton pair-correlation function vs distance at a temperature of $T=6$ K. The solid line refers to the calculated exciton-exciton potential for sample A. The dashed line represents ideal bosons, while the dot-dashed line holds for ideal fermions.

VIII. CONCLUSIONS

In the investigation of the many-exciton problem in semiconductor quantum structures, we have found a much richer spin structure with spatially dependent interaction potentials than with just contact interactions. This is due to nontrivial exchange processes of the fermionic constituents. For the spatially dependence of the potentials, we compared three different levels of approximation: The Hartree-Fock and the Heitler-London approximations as well as a newly introduced full numerical solution of the two exciton problem. We found a principal failure of the Hartree-Fock treatment, which is cured in the Heitler-London approach. The quality of the latter, however, turns out to be quite poor compared to numerically exact results. With our calculated potentials we have investigated bilayer systems and two different CQWs. The charge separation d plays a fundamental role: By tuning d a transition happens from systems with possible biexciton formation to those where biexcitons are not bound due to the stronger XX repulsion. For two realistic CQW structures, we have calculated the quasiparticle shift and broadening at the band edge which govern roughly the photoluminescence line shape. At low temperatures, we found a dramatic reduction of the blueshift compared to a naive treatment of the CQW as plate capacitor. The broadening turns out to be of the same order as the blueshift.

ACKNOWLEDGMENTS

Numerous stimulating discussions with Leonid Butov, Boris Laikhtman, Vincenzo Savona, and Dave Snoke are gratefully acknowledged.

APPENDIX

In the limit of infinitely heavy holes, the interaction part of the many-exciton Hamiltonian (Table II) can be written as[33]

$$\begin{aligned} H_{XX}^{\mathrm{int}} = & \frac{1}{2}\int d\mathbf{R}d\mathbf{R}'U^a(\mathbf{R}-\mathbf{R}') \\ & \times\sum_{ss'}\Psi_s^\dagger(\mathbf{R})\Psi_{s'}^\dagger(\mathbf{R}')\Psi_{s'}(\mathbf{R}')\Psi_s(\mathbf{R}) \\ & + \frac{1}{4}\int d\mathbf{R}d\mathbf{R}'[U^a(\mathbf{R}-\mathbf{R}')-U^s(\mathbf{R}-\mathbf{R}')]\sum_{ss'}\Theta(s\cdot s') \\ & \times[\Psi_{s'}^\dagger(\mathbf{R})\Psi_s^\dagger(\mathbf{R}')\Psi_{s'}(\mathbf{R}')\Psi_s(\mathbf{R}) \\ & - \Psi_s^\dagger(\mathbf{R})\Psi_{s'}^\dagger(\mathbf{R}')\Psi_{s'}(\mathbf{R}')\Psi_s(\mathbf{R}) \\ & + \Psi_{s'}^\dagger(\mathbf{R})\Psi_{-s'}^\dagger(\mathbf{R}')\Psi_{-s}(\mathbf{R}')\Psi_s(\mathbf{R})(1-2\delta_{ss'})]. \end{aligned} \tag{A1}$$

For the simplifications of contact potentials $U^p(\mathbf{R}-\mathbf{R}')=U^p\delta(\mathbf{R}-\mathbf{R}')$, our result agrees with the one derived by de-Leon and Laikhtman.[8] This can be seen as follows: Plugging the contact potentials into Eq. (A1) the integration over $\mathbf{R}'$ can be carried out immediately,

$$\begin{aligned} H_{XX}^{\mathrm{int}} = & \frac{1}{2}U^a\int d\mathbf{R}\sum_{ss'}\Psi_s^\dagger(\mathbf{R})\Psi_{s'}^\dagger(\mathbf{R})\Psi_{s'}(\mathbf{R})\Psi_s(\mathbf{R}) \\ & + \frac{1}{4}(U^a-U^s)\int d\mathbf{R}\sum_{ss'}\Theta(s\cdot s') \\ & \times\Psi_{s'}^\dagger(\mathbf{R})\Psi_{-s'}^\dagger(\mathbf{R})\Psi_{-s}(\mathbf{R})\Psi_s(\mathbf{R})(1-2\delta_{ss'}). \end{aligned} \tag{A2}$$

We can now drop the Heaviside step function by inserting a factor of 1/2 to account for the double counting in the sum over s and s' and get

$$\begin{aligned} H_{XX}^{\mathrm{int}} = & \frac{1}{2}U^a\int d\mathbf{R}\sum_{ss'}\Psi_s^\dagger(\mathbf{R})\Psi_{s'}^\dagger(\mathbf{R})\Psi_{s'}(\mathbf{R})\Psi_s(\mathbf{R}) \\ & + \frac{1}{8}(U^a-U^s)\int d\mathbf{R}\sum_{ss'}\Psi_{s'}^\dagger(\mathbf{R})\Psi_{-s'}^\dagger(\mathbf{R}) \\ & \times\Psi_{-s}(\mathbf{R})\Psi_s(\mathbf{R})(1-2\delta_{ss'}). \end{aligned} \tag{A3}$$

In the language of the Hartree-Fock approximation, we can trade the symmetric and the antisymmetric potentials for the direct and the exchange ones. For arbitrary hole masses, $U_d(\mathbf{R})$ and $U_x(\mathbf{R})$ have been derived in the literature.[6] For immobile holes they reduce to the direct potential,

$$\begin{aligned} U_d(\mathbf{R}) = & v_{hh}(\mathbf{R}) + \int d\mathbf{r}d\mathbf{r}'\phi^2(\mathbf{r})v_{ee}(\mathbf{r}-\mathbf{r}')\phi^2(\mathbf{r}'-\mathbf{R}) \\ & - 2\int d\mathbf{r}v_{eh}(\mathbf{r})\phi^2(\mathbf{r}-\mathbf{R}), \end{aligned} \tag{A4}$$

and the exchange potential,

$$\begin{aligned} U_x(\mathbf{R}) = & -\mathcal{O}^2(\mathbf{R})v_{hh}(\mathbf{R}) - \int d\mathbf{r}d\mathbf{r}'\phi(\mathbf{r})\phi(\mathbf{r}-\mathbf{R}) \\ & \times v_{ee}(\mathbf{r}-\mathbf{r}')\phi(\mathbf{r}')\phi(\mathbf{r}'-\mathbf{R}) \\ & + 2\mathcal{O}(\mathbf{R})\int d\mathbf{r}v_{eh}(\mathbf{r})\phi(\mathbf{r})\phi(\mathbf{r}-\mathbf{R}). \end{aligned} \tag{A5}$$

Taken in the contact limit $U^a=U_d+U_x$ and $U^s=U_d-U_x$, Eq. (A3) can be written as

$$\begin{aligned} H_{XX}^{\mathrm{int}} = & \frac{1}{2}U_d\int d\mathbf{R}\sum_{ss'}\Psi_s^\dagger(\mathbf{R})\Psi_{s'}^\dagger(\mathbf{R})\Psi_{s'}(\mathbf{R})\Psi_s(\mathbf{R}) \\ & + \frac{1}{4}U_x\int d\mathbf{R}\sum_{ss'}[2\Psi_s^\dagger(\mathbf{R})\Psi_{s'}^\dagger(\mathbf{R})\Psi_{s'}(\mathbf{R})\Psi_s(\mathbf{R}) \\ & + \Psi_{s'}^\dagger(\mathbf{R})\Psi_{-s'}^\dagger(\mathbf{R})\Psi_{-s}(\mathbf{R})\Psi_s(\mathbf{R})(1-2\delta_{ss'})]. \end{aligned} \tag{A6}$$

The Fourier transform of this result yields the Hamiltonian derived in Ref. 8.

*christoph.schindler@wsi.tum.de

[1] R. Knox, *Theory of Excitons*, Solid State Physics Suppl. 5 (Academic, New York, 1963).
[2] T. Usui, Prog. Theor. Phys. **23**, 787 (1960).
[3] L. V. Keldysh and A. N. Kozlov, Sov. Phys. JETP **27**, 521 (1968).
[4] E. Hanamura and H. Haug, Phys. Rep., Phys. Lett. **33**, 209 (1977).
[5] C. Ciuti, V. Savona, C. Piermarocchi, A. Quattropani, and P. Schwendimann, Phys. Rev. B **58**, 7926 (1998).
[6] J.-i. Inoue, T. Brandes, and A. Shimizu, Phys. Rev. B **61**, 2863 (2000).
[7] G. Rochat, C. Ciuti, V. Savona, C. Piermarocchi, A. Quattropani, and P. Schwendimann, Phys. Rev. B **61**, 13856 (2000).
[8] S. Ben-Tabou de-Leon and B. Laikhtman, Phys. Rev. B **63**, 125306 (2001).
[9] S. Okumura and T. Ogawa, Phys. Rev. B **65**, 035105 (2001).
[10] An early attempt including some features of the Heitler-London method to excitons is found in: A. I. Bobrysheva, Phys. Status Solidi **16**, 337 (1966).
[11] S. A. Moskalenko, Sov. Phys. Solid State **4**, 199 (1962).
[12] Y. E. Lozovik and V. I. Yudson, JETP Lett. **22**, 274 (1975).
[13] L. V. Keldysh and Y. V. Kopaev, Sov. Phys. Solid State **6**, 2219 (1965).
[14] L. V. Butov, A. Zrenner, G. Abstreiter, G. Böhm, and G. Weimann, Phys. Rev. Lett. **73**, 304 (1994).
[15] V. B. Timofeev, A. V. Larionov, M. Grassi-Alessi, M. Capizzi, and J. M. Hvam, Phys. Rev. B **61**, 8420 (2000).

[16] L. V. Butov, C. W. Lai, A. L. Ivanov, A. C. Gossard, and D. S. Chemla, Nature (London) **417**, 47 (2002).
[17] D. Snoke, S. Denev, Y. Liu, L. Pfeiffer, and K. West, Nature (London) **418**, 754 (2002).
[18] D. Snoke, Science **298**, 1368 (2002).
[19] R. Rapaport, G. Chen, and S. H. Simon, Phys. Rev. B **73**, 033319 (2006).
[20] G. Chen, R. Rapaport, L. N. Pffeifer, K. West, P. M. Platzman, S. Simon, Z. Voros, and D. Snoke, Phys. Rev. B **74**, 045309 (2006).
[21] Z. Voros, D. W. Snoke, L. Pfeiffer, and K. West, Phys. Rev. Lett. **97**, 016803 (2006).
[22] A. T. Hammack, M. Griswold, L. V. Butov, L. E. Smallwood, A. L. Ivanov, and A. C. Gossard, Phys. Rev. Lett. **96**, 227402 (2006).
[23] A. T. Hammack, L. V. Butov, L. Mouchliadis, A. L. Ivanov, and A. C. Gossard, Phys. Rev. B **76**, 193308 (2007).
[24] G. Aichmayr, M. Jetter, L. Viña, J. Dickerson, F. Camino, and E. E. Mendez, Phys. Rev. Lett. **83**, 2433 (1999).
[25] V. I. Sugakov, Solid State Commun. **134**, 63 (2005).
[26] C. S. Liu, H. G. Luo, and W. C. Wu, J. Phys.: Condens. Matter **18**, 9659 (2006).
[27] L. V. Butov, A. C. Gossard, and D. S. Chemla, Nature (London) **418**, 751 (2002).
[28] L. V. Butov, Solid State Commun. **127**, 89 (2003).
[29] D. Snoke, Y. Liu, S. Denev, L. Pfeiffer, and K. West, Solid State Commun. **127**, 187 (2003).
[30] D. A. Kleinman, Phys. Rev. B **28**, 871 (1983).
[31] R. C. Miller, D. A. Kleinman, A. C. Gossard, and O. Munteanu, Phys. Rev. B **25**, 6545 (1982).
[32] J. Usukura, Y. Suzuki, and K. Varga, Phys. Rev. B **59**, 5652 (1999).
[33] R. Zimmermann and C. Schindler, Solid State Commun. **144**, 395 (2007).
[34] R. Zimmermann, Phys. Status Solidi B **243**, 2358 (2006).
[35] S. Ben-Tabou de-Leon and B. Laikhtman, Europhys. Lett. **59**, 728 (2002).
[36] J. J. Forney, A. Quattropani, and F. Bassani, Nuovo Cimento **22**, 153 (1974).
[37] R. Zimmermann, Solid State Commun. **134**, 43 (2005).
[38] B. Laikhtman, J. Phys.: Condens. Matter **19**, 295214 (2007).
[39] M. Y. J. Tan, N. D. Drummond, and R. J. Needs, Phys. Rev. B **71**, 033303 (2005).
[40] R. M. Lee and R. Needs (private communication).
[41] S. de-Leon and B. Laikhtman, Phys. Rev. B **61**, 2874 (2000).
[42] D. W. Snoke, Y. Liu, Z. Vörös, L. Pfeiffer, and K. West, Solid State Commun. **134**, 37 (2005).
[43] R. Rapaport, G. Chen, D. Snoke, S. H. Simon, L. Pfeiffer, K. West, Y. Liu, and S. Denev, Phys. Rev. Lett. **92**, 117405 (2004).
[44] S. Yang, A. V. Mintsev, A. T. Hammack, L. V. Butov, and A. C. Gossard, Phys. Rev. B **75**, 033311 (2007).
[45] L. V. Butov, A. Imamoglu, A. A. Shashkin, V. T. Dolgopolov, A. V. Mintsev, S. Feklisov, K. L. Campman, and A. C. Gossard, Phys. Status Solidi A **178**, 83 (2000).
[46] V. Negoita, D. W. Snoke, and K. Eberl, Phys. Rev. B **61**, 2779 (2000).
[47] X. Zhu, P. B. Littlewood, M. S. Hybertsen, and T. M. Rice, Phys. Rev. Lett. **74**, 1633 (1995).
[48] S. A. Morgan, M. D. Lee, and K. Burnett, Phys. Rev. A **65**, 022706 (2002).